A&A, 679, A72 (2023)
https://doi.org/10.1051/0004-6361/202347676

Astronomy & Astrophysics

The $^{12}C/^{13}C$ isotopic ratio at the dawn of chemical evolution*

P. Molaro[1,2], D. S. Aguado[3,5], E. Caffau[4], C. Allende Prieto[3,5], P. Bonifacio[4], J. I. González Hernández[3,5], R. Rebolo[3,5,6], M. R. Zapatero Osorio[7], S. Cristiani[1,2], F. Pepe[8], N. C. Santos[9,10], Y. Alibert[16], G. Cupani[1,2], P. Di Marcantonio[1], V. D'Odorico[1,2,11], C. Lovis[8], C. J. A. P. Martins[9,13], D. Milaković[1,2,14], M. T. Murphy[2,17], N. J. Nunes[12], T. M. Schmidt[8,1], S. Sousa[9], A. Sozzetti[15], and A. Suárez Mascareño[3,5]

(Affiliations can be found after the references)

Received 8 August 2023 / Accepted 20 September 2023

ABSTRACT

Context. The known mega metal-poor (MMP) and hyper metal-poor (HMP) stars, with [Fe/H] < −6.0 and < −5.0, respectively, likely belong to the CEMP-no class, namely, carbon-enhanced stars with little or no second peak neutron-capture elements. They are likely second-generation stars, and the few elements measurable in their atmospheres are used to infer the properties of a single or very few progenitors.

Aims. The high carbon abundance in the CEMP-no stars offers a unique opportunity to measure the carbon isotopic ratio, which directly indicates the presence of mixing between the He- and H-burning layers either within the star or in the progenitor(s). By means of high-resolution spectra acquired with the ESPRESSO spectrograph at the VLT, we aim to derive values for the $^{12}C/^{13}C$ ratio at the lowest metallicities.

Methods. We used a spectral synthesis technique based on the SYNTHE code and on ATLAS models within a Markov chain Monte Carlo methodology to derive $^{12}C/^{13}C$ in the stellar atmospheres of four of the most metal-poor stars known: the MMP giant SMSS J0313−6708 ([Fe/H] < −7.1), the HMP dwarf HE 1327−2326 ([Fe/H] = −5.8), the HMP giant SDSS J1313−0019 ([Fe/H] = −5.0), and the ultra metal-poor subgiant HE 0233−0343 ([Fe/H] = −4.7). We also revised a previous value for the MMP giant SMSS J1605−1443 ([Fe/H] = −6.2).

Results. In four stars we derive an isotopic value while for HE 1327−2326 we provide a lower limit. All measurements are in the range $39 < {}^{12}C/^{13}C < 100$, showing that the He- and H-burning layers underwent partial mixing either in the stars or, more likely, in their progenitors. This provides evidence of a primary production of ^{13}C at the dawn of chemical evolution. CEMP-no dwarf stars with slightly higher metallicities show lower isotopic values, <30 and even approaching the CNO cycle equilibrium value. Thus, extant data suggest the presence of a discontinuity in the $^{12}C/^{13}C$ ratio at around [Fe/H] ≈ − 4 , which could mark a real difference between the progenitor pollution captured by stars with different metallicities. We also note that some MMP and HMP stars with high $^{12}C/^{13}C$ show low ^{7}Li values, providing an indication that mixing in the CEMP-no progenitors is not responsible for the observed Li depletion.

Key words. stars: abundances – stars: carbon – stars: individual: SDSS J1313-0019 – stars: individual: SMSS J0313-6708 – stars: individual: HE 1327-2326 – stars: individual: SMS J1605-1443

1. Introduction

Following the discovery of HD 140283 and HD 19445 by Chamberlain & Aller (1951), the search for metal-poor stars proceeded serendipitously or by selecting stars with anomalous kinematics with regard to the Galactic rotation (Bessell & Norris 1984). A breakthrough came in the 1980s with the H&K survey of Beers et al. (1985), who identified many metal-poor candidates with [Fe/H] ≈ −4 that were later confirmed by means of high-resolution follow-ups (Molaro & Castelli 1990; Molaro & Bonifacio 1990). The H&K survey revealed that a large fraction of metal-poor stars were enriched in carbon, the so-called carbon-enriched metal-poor (CEMP) stars. CEMP stars show the presence of neutron-capture (n-capture) elements, revealing the imprint of asymptotic giant branch (AGB) contamination. A puzzling CEMP star without any detectable presence of elements formed by the slow n-capture process, CS 22957-27, was found by Norris et al. (1997) and Bonifacio et al. (1998). These papers were submitted a few days apart. Other CEMP stars without signs of n-capture elements were found by Aoki et al. (2002), and Christlieb et al. (2004) discovered the remarkable HE 0107−5240 giant with [Fe/H] = −5.4, [C/Fe] > 3.9, and no detectable n-capture elements, from the Hamburg/ESO objective prism survey. These stars were grouped into the CEMP-no class, where the 'no' indicates the absence of n-capture elements, defined as stars with [C/Fe] > 0.7, originally >1.0, and [Ba/Fe]< 0.0; the more common stars with [Ba/Fe] > 1 are called CEMP-s, where 's' indicates the presence of n-capture elements (Beers & Christlieb 2005).

Spite et al. (2013) noted that [C/Fe] increases with decreasing iron, which implies a constant carbon abundance, and suggested two different nucleosynthetic origins for the carbon in the CEMP-no and CEMP-s stars. While in CEMP-s stars carbon is coming from an AGB companion along with the n-capture elements, in the CEMP-no stars the carbon was presumably already present in the gas from which the star formed (Spite et al. 2013; Bonifacio et al. 2015). Radial velocity studies have found that almost all CEMP-s stars are in binary systems, unlike CEMP-no stars, which supports this idea (Hansen et al. 2015, 2016).

Subsequent surveys such as the Sloan Digital Sky Survey (York et al. 2000) and its extensions SEGUE (Yanny et al. 2009) and SEGUE-2 (Rockosi et al. 2022), AEGIS (Keller et al. 2007),

* Based on ESPRESSO GTO observations collected under ESO programmes 1104.C-0350 and 108.2268.001 (PI: P. Molaro).

LAMOST (Deng et al. 2012), Pristine (Starkenburg et al. 2017), and TOPoS (Caffau et al. 2013) increased the number of known CEMP-no stars, showing that they dominate the low-metallicity tail. Metal-poor stars are defined as ultra metal-poor (UMP), hyper metal-poor (HMP), and mega metal-poor (MMP), corresponding to [Fe/H] < −4, [Fe/H] < −5, and [Fe/H] < −6, respectively. There are two MMP stars and seven HMP stars known to date, all of which are CEMP-no. There are also five known UMP stars with [Fe/H] < −4.5, three of which are CEMP-no and two are normal stars with approximately solar-scaled abundances (see Aguado et al. 2023 and references therein). Cooling of the gas by fine-structure line emission of singly ionised carbon or neutral atomic oxygen could have allowed the formation of CEMP-no stars earlier than those with normal carbon levels (Bromm & Loeb 2003). CEMP-s stars are seen only for [Fe/H] > −4.5, and this is likely because CEMP-s stars require the time necessary for the companion to evolve into an AGB star. It was also determined that CEMP-no stars are found primarily in the outer halo (Carollo et al. 2012), while a significant dearth of CEMP-no stars in the Galactic Bulge is interpreted as a signature of pair instability supernovae (SNe; Pagnini et al. 2023). Zepeda et al. (2023) found evidence that CEMP-no stars form chemo-dynamically tagged groups with a low dispersion in their [C/Fe] abundances.

The extremely low iron abundance of MMP and HMP stars suggests that only a few and perhaps just one single progenitor polluted the gas out of which they formed. The C enhancement could originate from faint SNe with energies of 10^{51} erg together with mixing and fallback (Umeda & Nomoto 2003, 2005; Nomoto et al. 2013; Tominaga et al. 2007, 2014). With a large amount of fallback, faint SNe eject a lot of carbon and a small amount of Fe. This produces ejecta with large [C/Fe] abundance ratios. An alternative model to explain the CEMP-no stars is represented by massive, low-metallicity fast-rotating stars called spinstars, with efficient mixing and mass loss (Meynet et al. 2006; Chiappini et al. 2008; Maeder et al. 2015; Limongi & Chieffi 2018). Therefore, the identification of the progenitors of CEMP-no stars has important bearings on the nature of the first stars (Frebel & Norris 2015). The elemental abundance pattern includes a limited number of elements, and the progenitors are poorly constrained. Thanks to their carbon enhancement, CEMP-no stars offer a unique opportunity to explore the behaviour of $^{12}C/^{13}C$ at the lowest metallicities. At low metallicities, very high $^{12}C/^{13}C$ ratios, greater than 10^3, are expected due to the secondary nature of ^{13}C (Chiappini et al. 2008; Romano & Matteucci 2003; Romano 2022; Kobayashi et al. 2020a). Aguado et al. (2022, 2023) derived significant bounds to the isotopic ratio $^{12}C/^{13}C$ in HE 0107−5240 and SMSS J1605−1443, with [Fe/H] = −5.8 and −6.2, respectively. In this paper we extend this analysis to four additional known extremely metal-poor (EMP) CEMP-no stars. We also reconsider the previous analysis of SMSS J1605−1443, for which new observations have since been conducted, and turn the bound into a value. We then discuss the results in the context of $^{12}C/^{13}C$ determinations in other CEMP-no stars, highlighting some implications that had until now been overlooked.

2. Observations and data reduction

Observations of some of the most metal-poor stars known have been taken with the ESPRESSO, the Echelle SPectrograph for Rocky Exoplanets and Stable Spectroscopic Observations, at the Very Large Telescope within the ESO Guaranteed Time Observations (GTO) programme on EMP stars (PI: Paolo Molaro).

Table 1. Journal of observations.

Star	MJD [(a)]	ESPRESSO mode	t_{exp} s	S/N 4300 Å
SMSS J0313−6708	58701.281	HR21	3400	12
SMSS J0313−6708	58732.245	HR21	3400	10
SMSS J0313−6708	58732.343	HR21	3400	14
SMSS J0313−6708	58740.153	HR21	3400	9
SMSS J0313−6708	58740.196	HR21	3400	8
SMSS J0313−6708	58742.119	HR21	3400	7
SMSS J0313−6708	58743.268	HR21	3400	15
SMSS J0313−6708	58743.335	HR21	3400	12
SMSS J0313−6708	58761.310	HR21	3400	14
SMSS J0313−6708	58793.309	HR21	3400	16
SMSS J0313−6708	59190.052	HR42	3417	20
SMSS J0313−6708	59237.078	HR42	3417	13
SMSS J0313−6708	59250.041	HR42	3417	11
SMSS J0313−6708	59264.017	HR42	3000	21
SMSS J0313−6708	59513.248	HR42	3000	23
SMSS J0313−6708	59882.103	HR42	3144	11
SMSS J0313−6708	59884.124	HR42	3144	17
HE 1327−2326	58615.137	HR21	1800	20
HE 1327−2326	58688.022	HR21	2700	23
HE 1327−2326	58688.055	HR21	2700	22
HE 1327−2326	58695.996	HR21	1800	25
HE 1327−2326	58697.988	HR21	2400	18
HE 1327−2326	58841.331	HR21	1800	23
HE 1327−2326	59429.054	HR42	3000	16
HE 1327−2326	59663.072	HR42	2844	41
HE 1327−2326	59990.288	HR42	3144	42
HE 0233−0343	58699.288	HR21	3400	10
HE 0233−0343	58760.318	HR21	3400	11
HE 0233−0343	58783.112	HR21	3400	14
HE 0233−0343	58813.243	HR21	3400	14
SDSS J1313−0019	59649.249	HR42	3444	12
SDSS J1313−0019	59972.310	HR42	3144	13
SDSS J1313−0019	60077.193	HR42	3144	9
SDSS J1313−0019	60080.092	HR42	3144	11
SDSS J1313−0019	60105.121	HR42	3144	12
SMSS J1605−1443	59676.277	HR42	3150	11
SMSS J1605−1443	59726.189	HR42	3150	11
SMSS J1605−1443	59727.060	HR42	3150	14
SMSS J1605−1443	59761.059	HR42	3150	10
SMSS J1605−1443	59792.055	HR42	3150	15
SMSS J1605−1443	60030.365	HR42	3144	10
SMSS J1605−1443	60078.265	HR42	3144	14

Notes. [(a)]Modified Julian date at the start of the observations.

The stars are SMSS J0313−6708, HE 1327-2326, HE 1313-0019 (also known as 2MASS J13132688-0019415), and HE 0233-0343 (also known as SDSS J002314.00+030758.0). Since a few additional observations for SMSS J1605−1443 were taken after the Aguado et al. (2023) analysis, we also revised the carbon isotopic ratio estimation for this star. The journal of the observations is given in Table 1 together with the ESPRESSO observing mode and the exposure times. The ESPRESSO spectrograph has two fibres, one for the target and one for the sky, with diameter of 140 μm that corresponds to a 1.″0 aperture on sky and provides a spectral coverage from 380.0 to 780.0 nm (Pepe et al. 2021). The CCD was binned by either 4 × 2 pixels (i.e. 4 pixels binned in the spatial direction and 2 in the spectral one) or by

2 × 1 pixels, as reported in the third column of Table 1. The corresponding resolution was $R = \lambda / \delta\lambda \approx 140.000$ for both binnings. The observations were performed in service mode with individual exposure times of the order of 3000 s. The precise exposure times and the signal-to-noise ratio per pixel measured at 4300 nm are provided in the last two columns of Table 1.

The automatic Data Reduction Software, DRS 3.0, of the ESPRESSO pipeline was used for the data reduction, which includes bias, flat-fielding correction, and sky subtraction, with the sky taken from the second fibre. The wavelength calibration combines a ThAr lamp with a Fabry-Pérot etalon as described in Pepe et al. (2013).

3. Analysis

3.1. The programme stars

In order to study the $^{12}C/^{13}C$ isotopic ratio at the beginning of chemical evolution, we selected some of the most metal-poor stars known. The sample includes the giant SMSS J0313−6708, discovered by Keller et al. (2014); with [Fe/H] < −7.3, it is the most iron-poor star presently known. We note that the inferred iron abundances are significantly higher in 3D non-local thermodynamic equilibrium than in 1D thermodynamic equilibrium, by 0.8 dex (Nordlander et al. 2017). The second most metal-poor giant is SMSS J1605−1443, first detected by the SkyMapper telescope; its iron abundance is measured at [Fe/H] = −6.2 by Nordlander et al. (2019). HE 1327−2326 with [Fe/H] = −5.60 is the most metal-poor turn-off star. It was discovered by Frebel et al. (2005, 2008) and studied by Aoki et al. (2006). The star has [Zn/Fe] = 0.8, and a 25 $M_\odot$ aspherical SN model exploding with $E = 5 \times 10^{51}$ erg has been suggested to provide the best match with the high zinc abundance (Ezzeddine et al. 2020). Our programme sample also includes the giant SDSS J1313−0019 with a measured metallicity of [Fe/H] = −5.0 ± 0.1. This star was discovered by Allende Prieto et al. (2015) and studied by Frebel et al. (2015) and Aguado et al. (2017). Allende Prieto et al. (2015) and Frebel et al. (2015) suggested that SDSS J1313−0019 could be a binary system. Finally, the sample includes another turn-off star, HE 0233−0343, with [Fe/H] = −4.68 ± 0.2 dex (Beers et al. 2007; García Pérez et al. 2008; Hansen et al. 2014). The carbon abundance in all these stars is A(C) ≈ 6−7, falling in the low-C band; although their barium abundance limits are not sensitive enough to match the condition [Ba/Fe] < 0, all of them can be classified as CEMP-no stars.

3.2. Carbon isotopic ratio $^{12}C/^{13}C$

Deriving $^{12}C/^{13}C$ ratios in metal-poor stars is challenging due to the weakness of the ^{13}C lines. However, the high carbon abundance of CEMP stars and the hundreds of lines of the *G* band collectively provide sufficient information (Masseron et al. 2014). Portions of the combined ESPRESSO spectra of the programme stars corresponding to the strongest ^{13}C lines are shown in Fig. 1. We computed stellar models using the ATLAS model atmosphere code assuming stellar parameters such as effective temperature ($T_{\rm eff}$), surface gravity ($\log g$), metallicity ([Fe/H]), and total carbon abundance, A(C). This code employs an opacity distribution function corresponding to a metallicity of −5.0[1].

The stellar parameters used in our analysis are those obtained from the most complete studies of the stars under study since there is no way to verify or improve them. The adopted stellar parameters for SMSS J0313−6708 are $T_{\rm eff}$ = 5125 ± 100 K and $\log g = 2.3 \pm 0.2$, as derived from low-resolution spectrophotometry by Keller et al. (2014). Those of HE 1327−2326 are $T_{\rm eff}$ = 6180 ± 100 K and $\log g$ = 3.70 ± 0.3, from Aoki et al. (2006). We note that Aoki et al. (2006) also find a solution for a slightly higher surface gravity of $\log g = 4.5 \pm 0.3$ with an almost equal probability that the star is a dwarf or a subgiant, though the *Gaia* parallax favours the subgiant solution. For HE 0233−0343, Hansen et al. (2015) obtained $T_{\rm eff}$ = 6100 ± 100 K and $\log g = 3.4 \pm 0.3$ dex, but the *Gaia* parallax suggests $T_{\rm eff}$ = 6230 and $\log g$ = 4.43. SDSS J1313−0019 has $T_{\rm eff}$ = 5200 ± 150 K and $\log g = 26 \pm 0.5$ ± according to Frebel et al. (2015). The stellar parameters of SMSS J1605−1443 are $T_{\rm eff}$ = 4850 ± 100 and $\log g$ = 2.0 ± 0.2 dex as derived by Nordlander et al. (2019). These stellar parameters are summarised in Table 2. We adopted an [α/Fe] ratio of +0.4 and microturbulences of 1.8, 2.0, 1.5, 1.5, and 1.5 km s^{-1} for SMSS J1605−1443, SMSS J0313−6708, SDSS J1313−0019, HE 0233−0343, and HE 1327−2326, respectively. It should be noted that line intensities of isotopic molecules originate from identical or very similar rotational and vibrational levels, making the isotope ratio relatively insensitive to uncertainties in the atmospheric parameters.

With this model atmosphere, we generated a grid of synthetic spectra using the SYNTHE code (Kurucz 2005; Sbordone 2005). We adopted the solar carbon abundance of $A(C)_\odot$ = 8.46 from Asplund et al. (2021). For each set of stellar parameters

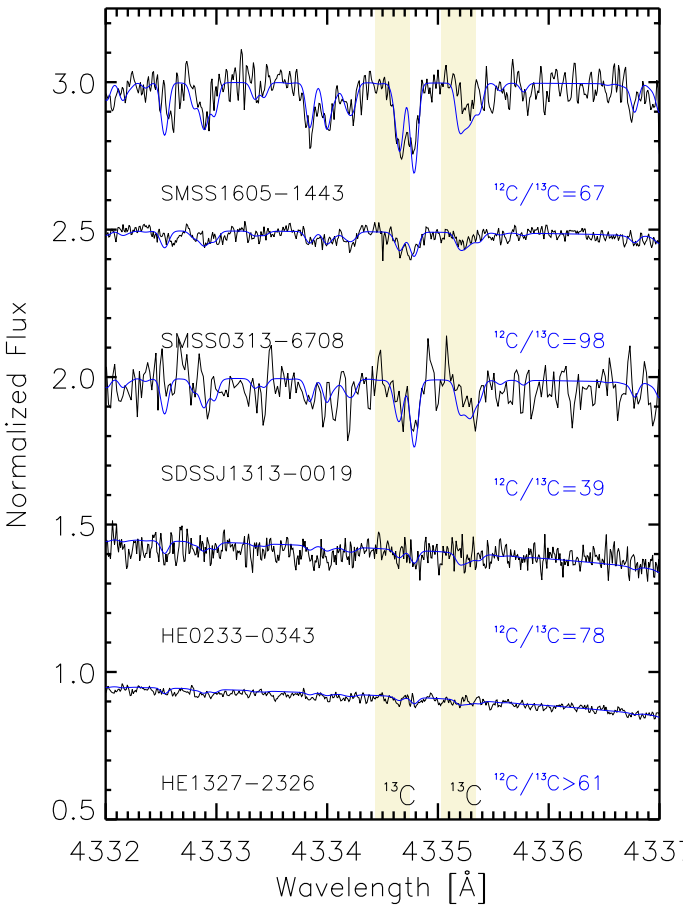

Fig. 1. Portion of the combined ESPRESSO spectra of the HMP stars, with a focus on the strongest lines of ^{13}C in the *G* band. The best fit derived with FERRE using an MCMC algorithm is displayed in magenta.

[1] https://wwwuser.oats.inaf.it/castelli/odfnew.html

Table 2. Abundance data for the CEMP-no stars grouped in bins of iron metallicity.

Star	$T_{\rm eff}$	log g	[Fe/H]	A(C)	A(Li)	$^{12}C/^{13}C$	[Sr/Fe]	[Ba/Fe]	Source
MMP									
SMSS J0313-6708	5125	2.3	<−7.1	6.06	**0.7±0.15**	**98.5±5.5**			1, 4
SMSS J1605-1443	4850	2.0	−6.21	6.81	**<0.0**	**67.3±1.0**	**<0.18**	**<0.6**	1, 6, 19
HMP									
HE 1327-2326	6180	3.7	−5.76	6.96	<0.62	**> 47**	+1.04	**1.3 ±0.2**	1, 2, 12
HE 0107-5240	5100	2.2	−5.56	6.75	<0.50	87.0±6	< −0.76	<0.2	2, 5, 12
SDSS J0023+0307	6140	4.8	<−5.5	6.20	+2.02 ±0.08				17, 21
SDSS J0815+4729	6050	4.6	−5.50	7.43	<1.3	-	<1.02	<1.91	18, 23
SDSS J1035+0641	6262	4.0	<−5.2	7.02	+1.90	-			13
SDSS J1313-0019	5200	2.6	−5.0	6.42	<0.8	**39.1±0.6**	<−0.28	<0.22	1, 15, 20
UMP									
SDSS J0929+0238	5894	4.5	−4.97	7.44	-	-	<0.70	<1.46	16
HE 0557-4840	4900	2.2	−4.81	5.35	-	-	<0.0	<−1.0	12
SDSS J1742+2531	6345	4.0	−4.80	7.26	<1.8	-	<0.72	<1.56	14
HE 0233–0343	6230	4.43	−4.70	7.24	**+1.65±0.2**	**78.9± 5.4**	+0.3	<0.8	1, 7
SDSS J1442-0015	5850	4.0	−4.37	6.02	<1.58	-			13
HE 1310–0536	5000	1.9	−4.20	6.62	<0.8	3	−1.08±0.14	−0.50±0.15	7
HE 0057-5959	5257	2.65	−4.08	5.24	-	>2		−0.46	12
SDSS J0140+2344	5703	4.68	−4.05	5.76	+1.86	>2	+1.09	<0.34	12,13
G77-61	4000	5.05	−4.03	7.01	<1.0	5±1		<1.0	2, 3
HE 2139-5432	5416	3.04	−4.02	7.03	-	>15		<–0.33	12
SDSS J1034+0701	6224	4.0	−4.01	6.28	+2.24	-			13
SDSS J1247-0341	6224	4.0	−4.01	6.64	+2.2:	-			13
HE 0134–1519	5500	3.2	−4.00	5.46	-	>4	−0.30±0.19	<−0.50	7
EMP									
CS 22949-037	4958	1.84	−3.97	5.55	<0.13	4±1	+0.55	−0.52	3,12
HE 1201-1512	5725	4.67	−3.89	5.94	-	>20		<−0.34	12
HE 1300+0157	5529	3.25	−3.75	6.02	+1.0±0.09	>3		<−0.85	12, 2
HE 2331–7155	4900	1.5	−3.70	6.10	-	5	−0.85±0.20	−0.90±0.21	7
BD +44 493	5510	3.70	−3.68	6.09	+0.64	-		−0.60	12
CS 22885-096	5050	1.9	−3.66	5.40	<0.5	-		−1.64	2
SDSS J1349+1407	6112	4.0	−3.60	6.82	<0.9	-			13
HE 1506-0113	5016	2.01	−3.54	6.39	+1.01±0.09	>20		−0.80	12
Segue 1-7	4960	1.90	−3.52	7.24	-	>50			12
CS 29498-043	4639	1.00	−3.49	6.87	-	6±2			2, 12
HE 0146-1548	4636	0.99	−3.46	6.08	-	4		−0.71	12
HE 1150-0428	5208	2.54	−3.47	7.36	-	4		−0.54±0.14	2,12
CS 30322-023	4100	0.3	−3.39	5.87	-	4			2,3
BS 16929-005	5229	2.61	−3.34	6.11	-	>7		−0.41	12
CS 22957-027	5170	2.45	−3.19	7.54	-	8±2		−1.23±0.21	9,10,8
LAMOST J1410-0555	6169	4.21	−3.19	6.80	+2.17		−0.10	−0.33	22
HE 1419-1324	4900	1.80	−3.05	7.17	-	12±2		+0.88±0.1	2,3
SDSS J1424+5615	6088	4.34	−3.01	6.94	+2.14	-	−0.40	<−0.69	22
HE 0100–1622	5400	3.0	−2.90	8.31	<1.12	13	+0.25±0.25	<−1.80	7
MP									
CS 29502-092	5074	2.21	−2.99	6.43	<1.2	20		−1.36±0.07	12, 2
HE 2247-7400	4929	1.56	−2.87	6.29	-	-		−0.94	12
CS 22958-042	6250	3.5	−2.85	8.76	<0.6	9±2		−0.53±0.16	2,3, 11
CS 30314-067	4400	0.7	−2.85	6.11	<0.6	-		−0.25	2
CS 31080-095	6050	4.5	−2.85	8.30	+1.73 ±0.05	>40			2,3,11
CS 22877-001	5100	2.2	−2.72	6.74	<1.2	>10		−0.51	2,3,8
HE 2319-5228	4900	1.6	−2.60	7.56	-	5			7
CS 22945-017	6400	3.80	−2.52	8.22	-	6±3		0.55±0.2	2,3
HE 1410+0213	4890	2.00	−2.52	8.27	-	3±0.5		+0.05±0.20	3
CS 22956-028	6700	3.50	−.33	7.97	-	5±2		+0.16±0.2	3
CS 22887-048	6500	3.7	−1.75	8.17	-	3			8

Notes. Mega metal-poor (MMP) stars with [Fe/H] < −6.0, hyper metal-poor (HMP) stars with [Fe/H] < −5.0, ultra metal-poor (UMP) stars with [Fe/H] < −4.0, extremely metal-poor (EMP) stars with [Fe/H] < −3.0, and metal-poor (MP) stars with [Fe/H] < −1.5. The table lists the CEMP-no stars presently known for which either the carbon isotopic ratio or the Li has been measured in the literature. In boldface are the new measurements presented in this paper. Limits are at the 3σ CL.

References. 1. This paper; 2. Allen et al. (2012); 3. Masseron et al. (2010); 4. Keller et al. (2014), 5. Aguado et al. (2022), 6. Aguado et al. (2023), 7. Hansen et al. (2015), 8. Aoki et al. (2002), 9. Bonifacio et al. (1998), 10. Norris et al. (1997), 11. Sivarani et al. (2006), 12. Norris et al. (2013a), 13. Bonifacio et al. (2018), 14. Bonifacio et al. (2015), 15. Allende Prieto et al. (2015), 16. Caffau et al. (2016), 17. Aguado et al. (2019), 18. Aguado et al. (2018), 19. Nordlander et al. (2019), 20. Frebel et al. (2015), 21. Frebel et al. (2019), 22. Matsuno et al. (2017), 23. González Hernández et al. (2020).

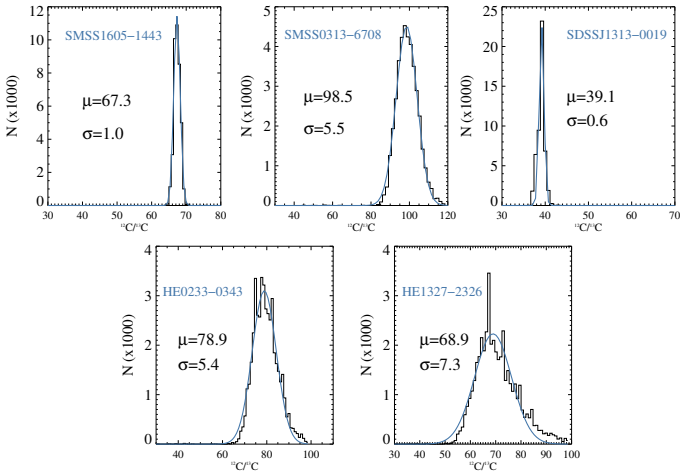

Fig. 2. Distribution of the MCMC experiments versus the most likely $^{12}C/^{13}C$ value for each of the targets. The mean value and typical deviation are displayed to provide a summary of the results.

corresponding to our targets, we computed models with varying $^{12}C/^{13}C$ ratios: 2.2, 5.3, 11.6, 24.1, 49.1, 99.0, and 198.6. These ratios were specifically chosen to capture the largely non-linear behaviour of $^{12}C/^{13}C$ ratios. With the SYNTHE stellar models, a grid in a format compatible with the FERRE code was constructed (Allende Prieto et al. 2006)[2]. We generated one grid per target, allowing the FERRE code to read and process the data seamlessly.

In Aguado et al. (2023) we tested a Markov chain Monte Carlo (MCMC) technique that enables the derivation of $^{12}C/^{13}C$ ratios even with marginal detections of the ^{13}C lines. This methodology is described in Appendix B of Aguado et al. (2023). In short, we identified the spectral regions of the *G* band near 430.0 nm, where the ^{13}C information is maximum, by subtracting two theoretical models with high and low $^{12}C/^{13}C$, respectively. This enabled us to concentrate the fitting procedure of the code exclusively on the pertinent regions while disregarding other features or minor artefacts present in the data. After a 300-pixel running-mean normalisation, the code employs an MCMC self-adaptive randomised subspace sampling algorithm for the fitting, which is described in Vrug et al. (2009). Ten chains of 5000 experiments each were run following this MCMC methodology. Based on our experience with the code, experiments from the initial chain can encounter a blockage. To address this, we allowed the algorithm to ignore the first 500 iterations. Finally, the code provides us with the most probable result and the samples from the Markov chains, following the approach used in Aguado et al. (2023). The sample distributions of the MCMC experiments versus the most likely $^{12}C/^{13}C$ value are shown in Fig. 2. In Fig. 1 the best FERRE fits are compared with the data in the region around ∼422.5 nm at the edge of the *G* band, where the strongest ^{13}C absorptions are.

We successfully measured the $^{12}C/^{13}C$ ratios in the three relatively cool giants. For the two MMP stars – SMSS J0313−6708 and HE 1605-1443 – the $^{12}C/^{13}C$ ratios are 98.5 ± 5.5 and 67.3 ± 1.0, respectively. Previously, Aguado et al. (2023) had set a lower limit of $^{12}C/^{13}C > 60$ for HE 1605-1443. In the HMP SDSS J1313−0019, the $^{12}C/^{13}C$ ratio is 39.1 ± 0.6. For the two relatively warm and unevolved stars, HE 1327-2326 and HE 0233−0343, the code provides $^{12}C/^{13}C$ ratios of 68.9 ± 7.3 and 78.9 ± 5.4, respectively. However, in the spectrum of HE 1327-2326, only very faint evidence of the ^{13}C lines can be observed by eye in Fig. 1. Thus, we conservatively considered a lower limit of 47 for this star at the 3σ confidence level (CL). Overall, all the CEMP-no stars investigated in this study exhibit $^{12}C/^{13}C$ values or lower limits in the range $39 < ^{12}C/^{13}C < 100$, providing evidence of primary production of ^{13}C at the dawn of chemical evolution.

[2] Available at http://github.com/callendeprieto/ferre

4. Discussion

The $^{12}C/^{13}C$ ratio is a solid indicator of the presence of CNO-cycle-processed material at the surface of a star. This processed material could come from the interior of the star or from the progenitors that polluted the gas from which the star formed. ^{12}C is formed in the triple-α process during hydrostatic helium burning and is a primary product of stellar nucleosynthesis. The stable ^{13}C isotope is produced in the hydrogen-burning shell when the CN cycle converts pre-existing ^{12}C into ^{13}C via proton capture followed by β decay. The $^{12}C/^{13}C$ is not locked to the C abundance and provides independent information on either the evolution of the star or the nature of the progenitor.

As a star evolves off the main sequence, the outer convective envelope expands inwards into the CN-cycle-processed regions. This mixing episode, called the 'first dredge-up', lowers the $^{12}C/^{13}C$ ratio from the original value (Iben & Renzini 1984).

Mixing also occurs in the thermal pulses of intermediate-mass stars that become AGB stars. This could lead to a CN-cycle equilibrium ratio of about $^{12}C/^{13}C \sim 3.4$, and in fact ratios as small as 6 are observed in the atmospheres of red supergiants (Lambert & Sneden 1977; Dearborn et al. 1975).

Nova explosions at temperatures $>10^8$ K can produce ^{13}C in a hot CNO cycle. Pre-nova white dwarfs are rich in CNO nuclei, and the hot CNO cycle triggers the explosion and transmutes CNO into ^{13}C, ^{15}N, and ^{17}O with enhancement factors of 100 times the solar values (Starrfield et al. 1972; José & Hernanz 1998). All stars as small as 1 solar mass can thus release matter enriched in ^{13}C into the interstellar medium via stellar wind or at the end of their evolution. Therefore, chemical evolution models predict a monotonic decrease in the isotopic ratio $^{12}C/^{13}C$ with time (Romano & Matteucci 2003; Kobayashi et al. 2020b). In fact, the value found in the interstellar medium and in young molecular clouds is $^{12}C/^{13}C \sim 60–70$, which is lower than the solar ratio, $^{12}C/^{13}C = 91 \pm 1.3$ (Goto et al. 2003; Ayres et al. 2013). Moreover, relatively low values of about 24 have been derived in the Galactic centre by Halfen et al. (2017), and a gradient is observed as a function of galactocentric distances that clearly shows the secondary nature of ^{13}C (Yan et al. 2023).

At low metallicities or before the birth of the Solar System, the $^{12}C/^{13}C$ is predicted to be higher than solar (Romano & Matteucci 2003; Chiappini et al. 2008; Kobayashi et al. 2020a; Romano 2022). This prediction is difficult to verify because there are few observations that can measure ratios higher than, or even close to, solar. Botelho et al. (2020) in 63 solar twins found a value close to solar with a mild increase in the metallicity range $-0.2 < [Fe/H] < -0.0$, which is opposite to what is expected. By contrast, Crossfield et al. (2019) measured $^{12}C/^{13}C = 296 \pm 45$ and 224 ± 26 in the two components of the brown dwarf system GJ 745 at [Fe/H] = −0.48, which are too high for the Galactic chemical evolution models. At lower metallicities, the isotopic ratio in metal-poor giants is found in the range 30–50 and in the metal-poor dwarf HD 140283 is $^{12}C/^{13}C = 33^{+12}_{-6}$ (Spite et al. 2006, 2021). Overall, observations do not provide a comprehensive evolutionary curve of the $^{12}C/^{13}C$ in the Galaxy.

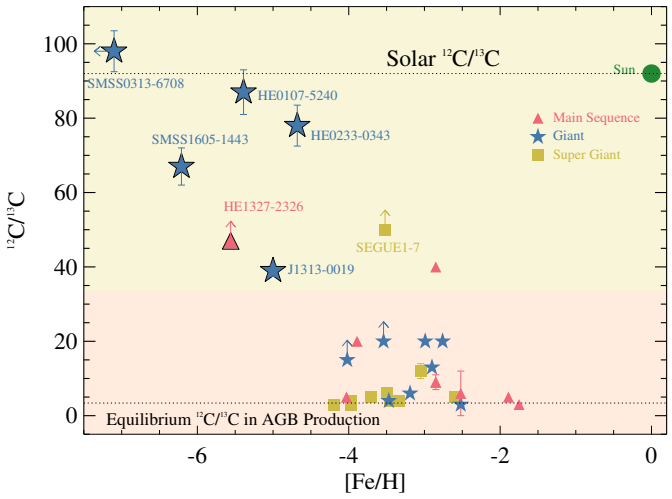

Fig. 3. $^{12}C/^{13}C$–[Fe/H] plane for CEMP-no stars. The value for HE 0107−5240 is taken from Aguado et al. (2022). Only lower limits greater than 15 are shown since the smaller ones do not provide useful information. Errors in [Fe/H] are omitted for clarity. Red triangles are dwarfs with $\log g > 3.5$. Blue star-symbols are stars on the first ascent to the red giant branch, with $2 < \log g < 3.5$. Orange squares are supergiants with $\log g < 2$. The $^{12}C/^{13}C = 30$ value that splits stars with evidence of internal mixing from the others according to Spite et al. (2006) is also shown; the background above this value is yellow and below is peach coloured.

In Fig. 3 we compile the existing $^{12}C/^{13}C$ measurements or significant limits of CEMP-no stars from the literature. Data are from Bonifacio et al. (1998), Aoki et al. (2002), Masseron et al. (2012), Norris et al. (2013b), Hansen et al. (2015), and Aguado et al. (2022, 2023). Only lower limits in $^{12}C/^{13}C$ greater than 15, which help in differentiating between low and high isotopes ratios, are shown. The majority of the CEMP-no stars in Fig. 3 have low $^{12}C/^{13}C$ values. The CEMP-no supergiants have $^{12}C/^{13}C < 10$, and the second dredge-up could have internally synthesised ^{13}C. However, quite remarkably there are low values in four dwarfs that have not gone through the first or second dredge-up. They are CS 22958-042 with $^{12}C/^{13}C = 4.5$ measured by Sivarani et al. (2006), CS 22887-048 with $^{12}C/^{13}C = 3.7$ measured by Aoki et al. (2002), CS 22956-028 with $^{12}C/^{13}C = 4.3$ measured by Masseron et al. (2010), and G77-61 with $^{12}C/^{13}C = 5$ measured by Plez & Cohen (2005). A chemical transfer from a possible massive companion can be ruled out since all these stars are single or belong to non-interacting binaries, and unless they are wrongly classified as CEMP-no stars, the enhancement of ^{13}C needs to come from their progenitors. This is probably also true for some giants that show very low $^{12}C/^{13}C$ values that cannot be the result of the first dredge-up. Already in the CEMP-no prototype CS 22957-027, the $^{12}C/^{13}C$ ratio is 10 ± 5, and Bonifacio et al. (1998) pointed out that the star's low luminosity means that the ^{13}C could not come from self-polluting dredge-up processes and that the absence of n-capture elements is evidence against mass transfer from an AGB companion.

We note that these measurements point to a complex Galactic behaviour for the ratio $^{12}C/^{13}C$. If it is very low at metallicities $-3.5 <$[Fe/H]< -2, then it needs to rise to match the solar value. This implies that the sources of primary ^{13}C should cease their contribution around [Fe/H] ≈ -2. If so, when the ^{12}C abundance increases by two orders of magnitude, the $^{12}C/^{13}C$ ratio would also increase by the required two orders of magnitude. Unfortunately, the lack of $^{12}C/^{13}C$ ratio measurements in the range $-2.0 <$ [Fe/H] < 0 prevents us from verifying this prediction. These measurements would have to be extended to other CEMP-no main-sequence stars to see if the low isotope ratios are common at low metallicities and trace the rise of the isotope ratio until it reaches the solar value.

Remarkably, all the MMP and HMP CEMP-no stars have $^{12}C/^{13}C > 40$, while the majority of other CEMP-no have values <30. There is also a hint of a smooth decrease in the values going from the MMP to the HMP stars and then to the UMP stars. In the sample of UMP and EMP stars, there are 30 CEMP-no stars and all but two of them show low $^{12}C/^{13}C$ ratios, in a few cases close to the CNO equilibrium value. The exceptions are Seque1−7 and CS31080-095, which have values of $^{12}C/^{13}C > 50$ and 40, respectively, which is comparable to the more metal-poor stars.

The extremely low iron abundance of MMP and HMP stars suggests that only a few and perhaps only a single progenitor polluted the gas out of which they formed. The carbon might originate from faint SNe with energies of 10^{51} erg (Umeda & Nomoto 2003). With mixing and a large amount of fallback, faint SNe eject a lot of carbon and a small amount of Fe, thus producing ejecta with large [C/Fe] abundance ratios. Supernovae with stellar masses of 10–20 $M_\odot$ and low explosion energies of about 10^{51} erg have been shown to be able to reproduce the pattern of chemical abundances of CEMP-no stars (Tominaga et al. 2014; Almusleh et al. 2021). Tominaga et al. (2007) successfully reproduced the observed abundance pattern of the CEMP-no star CS 29498-043 (Aoki et al. 2004) with a 25 $M_\odot$ faint SN model. Almusleh et al. (2021) suggest that weak SN progenitors with stellar masses of 11–22 $M_\odot$ and explosion energies in the range $0.3–1.8 \times 10^{51}$ erg could be the progenitors of the chemical abundances of five CEMP-no stars. However, models are not unique, and, for instance, several different kinds of progenitors with masses in the range 12–60 $M_\odot$ (Ishigaki et al. 2014; Nordlander et al. 2017) have been proposed to explain the abundances of the most iron-poor star known, SMSS J0313−6708. Moreover, a large dispersion in the [Fe/Ca] values is predicted by fallback models, which is not observed (Ishigaki et al. 2014). A variant model includes a double source with the CNO elements synthesised by faint SNe and the heavier elements made by conventional core-collapse SNe (Limongi et al. 2003; Bonifacio et al. 2015).

An alternative, potentially complementary, model for the progenitors of CEMP-no stars is massive low-metallicity, fast-rotating stars in the range 40–120 $M_\odot$, the so-called spinstars, which may experience efficient mixing and significant mass loss (Meynet et al. 2006; Chiappini et al. 2008; Maeder et al. 2015; Limongi & Chieffi 2018). Mixing is driven by rapid rotation, and the diffusion of matter between the H- and He-burning zones largely increases the abundance of ^{13}C. If ^{13}C flows into the convective core, it is transported to the surface and delivered into the interstellar medium by winds (Meynet et al. 2006; Chiappini et al. 2008; Maeder et al. 2015; Limongi & Chieffi 2018). In the spinstar model, the mixing occurs progressively during the evolutionary stages and ^{13}C is lost through stellar winds, while in the faint SN model the mixing that produces ^{13}C should occur in the explosion and is unconstrained.

High $^{12}C/^{13}C$ values imply partial or very mild mixing that occurred either within the star itself or in the progenitor. For the unevolved stars HE 1327−2326 and HE 0233−0343, all the ^{13}C is coming from the parent cloud. Generalising this result to the giants, it follows that the parent generation of the most metal-poor stars, likely the first stars, synthesised significant amounts of primary ^{13}C. A transition seems to occur at [Fe/H] ≈ -4 and

suggests the presence of different progenitors for the two groups of stars. The first generation of massive stars that polluted the gas seems to have made less ^{13}C than later generations.

Primordial faint SN models do not make specific predictions concerning the production of ^{13}C, while significant quantities of ^{13}C are expected from massive, low-metallicity, fast-rotating stars with ^{12}C/^{13}C ratios between 30 and 300 (Chiappini et al. 2008). In the zero-metallicity non-rotating stars models by Limongi & Chieffi (2012), the production of primary ^{13}C, and all CNO isotopes more generally, occurs in a restricted mass range between 25 and 35 $M_{\odot}$, where the convective shell of He, in which ^{12}C is produced from the He burning, incorporates the H shell. Once the He shell begins to engulf H, it extends considerably. The maximum extension of the shell is for a star of 25 $M_{\odot}$; for more massive stars it decreases and therefore the abundance of ^{13}C also decreases. Stars of 20 $M_{\odot}$ or 50 $M_{\odot}$ do not have this mixing and there is no production of ^{13}C. This picture could explain the observed trend with the more massive stars being the parents of the HMP stars and progressively lower-mass stars progenitors of the UMP stars. However, the presence of significant rotation could drive extra mixing in layers that are otherwise in radiative equilibrium. A rotational-driven mixing could bring the ^{12}C synthesised in the He convective core up into the tail of the H-burning shell, where it is converted into ^{13}C. However, the production is not monotonic due to a complex interplay between rotation and convection (Limongi 2023, priv. comm.). We note that similar processes necessary to produce ^{13}C are also invoked to explain the primary N behaviour at very low metallicities in damped Lyα galaxies (Molaro 2003; Molaro et al. 2004; Zafar et al. 2014).

4.1. n-capture elements

The CEMP-no classification does not imply a complete absence of n-capture elements, only that [Ba/Fe] < 0 (Christlieb et al. 2004). For the most iron-poor stars (i.e. [Fe/H] < −5), this condition is difficult to fulfil and limits are much less stringent. There are several cases where neither Ba nor Fe can be measured, leaving the [Ba/Fe] unconstrained. For instance, for SMSS J0313-6708 we can place [Ba/H] < −5.6 and [Sr/H] < −5.8, but the [Ba,Sr/Fe] ratios remain unbound. For these stars, the criterion for CEMP-no membership is necessarily restricted to the absolute carbon abundance, which for CEMP-no stars is around A(C) ≈ 6.8 ± 0.5 (Bonifacio et al. 2015). For SMSS J1605−1443, which has [Fe/H] = −6.21, Nordlander et al. (2019) in their discovery paper derived [Sr/Fe] < 0.2 and [Ba/Fe] < 1.0. With our ESPRESSO data we slightly improve upon these limits, placing an upper bound of [Sr/Fe] < 0.18 and [Ba/Fe] < 0.6 at the 3σ CL. In HE 1327-2326 and HE 0233−0343, strontium has been measured and found to be relatively abundant, with [Sr/Fe] = 1.04 and 0.3, respectively (Frebel et al. 2005; Hansen et al. 2014). The portion of the ESPRESSO spectrum of HE 1327-2326 corrected for a radial velocity of 63.681 km s^{-1} around the Ba II 455.40 nm line is shown in Fig. 4; it shows a hint of a line at the expected position. The abundance would be [Ba/Fe] = 1.3. Strictly speaking, this abundance violates the condition of [Ba/Fe] < 0.0. However, the star shows an absolute carbon abundance of A(C) = 6.96, similar to the other CEMP-no stars. Indeed, there is a small group of CEMP-no stars with measurable Sr, and some of them also have barium measured. With the present detection, HE 1327-2326 would be the CEMP-no star with the highest barium abundance relative to iron. The existence of this group of stars shows that n-capture elements sometimes need to be synthesised at a solar ratio

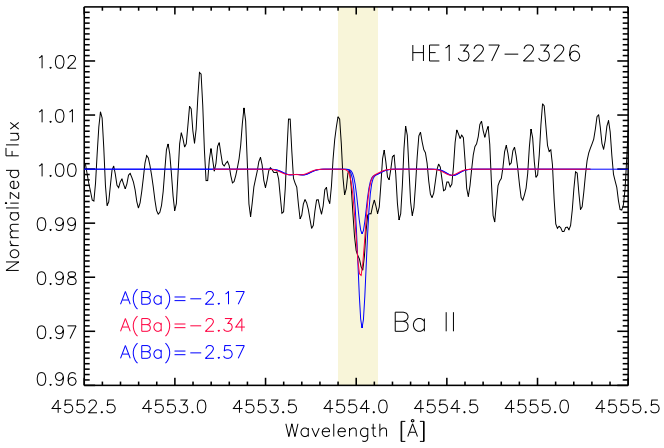

Fig. 4. ESPRESSO spectrum of HE 1327-2326 around the Ba II 455.40 nm line. Three different synthetic models computed with SYNTHE are also shown.

relative to iron from the very beginning. This may favour the scenario that foresees the additional contribution from core-collapse SNe in addition to faint SNe, though the latter are required to provide the seed nuclei. For high rotation velocities, the mixing processes with successive back and forth motions between the He- and H-burning layers may also lead to the ^{22}Ne(α,n)^{25}Mg reaction that produces s-elements by n-captures on seed heavy elements. In this way, a substantial number of s-elements of the first peak, such as Sr, corresponding to the magic number of neutrons N = 50, are formed, as are a few elements of the second peak, such as Ba, corresponding to the magic number of N = 82; nothing of the third peak is formed (Frischknecht et al. 2016).

4.2. Lithium in the CEMP-no stars

In the sample of stars with [Fe/H] < − 4.5, there are six unevolved stars with effective temperatures between 5800 and 6345 K. As noted by Sbordone et al. (2010), they should lie on the Spite and Spite plateau at metallicities below [Fe/H] = −3. The HMP and UMP stars follow this trend and magnify the meltdown, showing more Li-depleted stars at the lowest-metallicity end. Below [Fe/H] < −4.0 there are no stars with Li abundances strictly on the plateau, and about half of them show no detectable Li at all. This is in contrast with the recent suggestion by Heger & Woosley (2020), of significant Li production by neutrino-induced spallation during the explosion of very compact zero-metal core-collapse SNe. The ^{12}C/^{13}C values could also help in interpreting the origin of Li depletion. A clear correlation between ^{12}C/^{13}C and Li abundance is observed in a large sample of disk giants, with the low values in the isotopic ratio showing the highest Li depletion (Takeda et al. 2019). Stars with evidence of mixing also show Li depletion since Li is burned in the mixing process. This seems to also hold for the CEMP-no stars. One example is the CEMP-no dwarf CS 22958-042 with ^{12}C/^{13}C = 9 and A(Li) < 0.6 (Sivarani et al. 2006). However, HE 1327−2326 has A(Li) < 0.62 according to Frebel et al. (2005), which is considerably below the plateau value of A(Li) ≈ 2.2, but has a relatively high value of ^{12}C/^{13}C. This suggests that the mechanism behind the Li depletion is not mixing in the progenitor. Matsuno et al. (2017) also measured Li at the Spite plateau level in two CEMP-no stars with metallicities of about −3.0, arguing that the nature of neither the CEMP-no stars

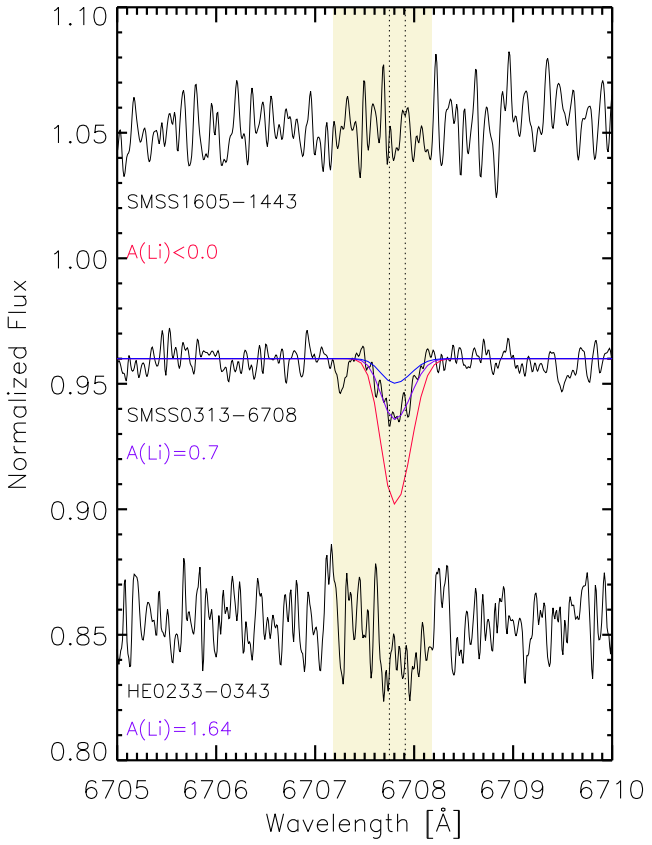

Fig. 5. ESPRESSO spectra for three representative stars around the Li 670.7 nm position. Radial velocities given in Aguado et al. (2022) have been subtracted.

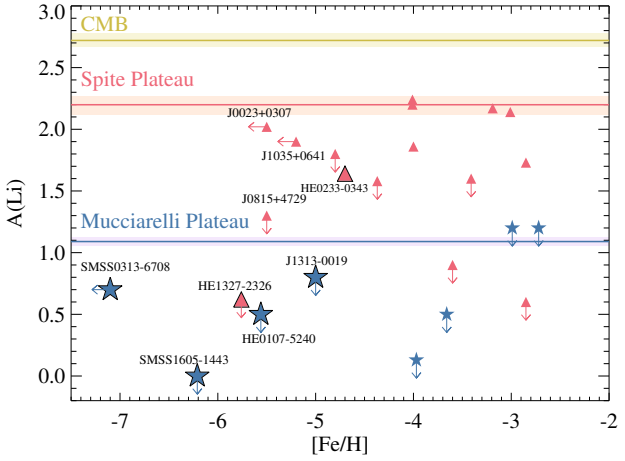

Fig. 6. Lithium abundances for CEMP-no stars from Table 2. The two plateaux for dwarfs and giants observed at higher metallicities are shown in red and blue, respectively. The former is from Sbordone et al. (2010), and the latter is at A(Li) = 1.09 ± 0.01 and is from Mucciarelli et al. (2022). Red triangles are for warm dwarfs, $T_{\rm eff} > 5800$ K and $\log g > 3.4$. Blue stars are for giants, $\log g < 3.0$. Supergiants with $\log g < 2.0$ are not shown.

nor their progenitors can explain the higher fraction of Li depletion at low metallicities. The mechanism seems more related to the metallicity, rather than the nature, of the CEMP-no stars or their progenitors.

A similar argument can also be made for the giants. Mucciarelli et al. (2022) find a thin Li plateau at A(Li) = 1.09 ± 0.01 in the giants following the Li dilution, which occurs when the star leaves the main sequence. It is quite remarkable that in SMSS J0313−6708, the most iron-poor star presently known, we measure A(Li) = 0.70 ± 0.15, see Fig. 5, in agreement with the 0.7 quoted by Keller et al. (2012). After correcting this value using the dilution factor from Mucciarelli et al. (2022), the original Li becomes 0.39 dex below the primordial value, regardless of whether this is at the Planck value of A(Li) ≈ 2.7 or at the halo stars' value of A(Li) ≈ 2.2. Thus, Li values below Mucciarelli's plateau indicate the presence of effective Li depletion. In the case of SMSS J1605−1443, we could place 3σ upper limits at A(Li) < 0.0, see Fig. 5, improving upon the A(Li) < 0.48 limit from Nordlander et al. (2019), as illustrated in Fig. 6 in the three giants with high ^{12}C/^{13}C, Li is observed at A(Li) < 0.6; this is below the Mucciarelli plateau, indicating Li depletion in excess of dilution.

Fu et al. (2015) suggest a stellar fix to the cosmological Li problem that involves a substantial pre-main-sequence depletion partially compensated for by gas accretion with a primordial Li composition of A(Li) = 2.7, as inferred from standard Big Bang nucleosynthesis, once the baryon density from the cosmic microwave background power spectrum or the D/H extragalactic measurements is adopted. The presence of overshooting, which is required by helioseismology, leads to a substantial Li burning in the pre-main-sequence evolution, which needs to be compensated for with a later accretion (Fu et al. 2015). An accretion rate of $10^{-8} M_0$ yr^{-1} at the birth line that then decays exponentially until it is halted by photo-evaporation provides a self-regulating mechanism able to reproduce a Li plateau for a range of stellar masses. The MMP and HMP stars are smaller and hotter, and the tenuous accretion disk could be dissipated before the restoration of the initial Li is completed. Thus, a break of this self-regulating mechanism could explain, at least qualitatively, the increased scatter of the lithium abundances at very low metallicities.

5. Conclusions

By means of high-resolution spectra acquired with the ESPRESSO spectrograph at the VLT, we succeeded in measuring the ^{12}C/^{13}C ratio in four of the lowest-metallicity stars known: the MMP giant SMSS J0313−6708, with [Fe/H] < −7.1; the HMP dwarf HE 1327−2326, [Fe/H] = −5.8; the giant SDSS J1313−0019, [Fe/H] = −5.0; and the UMP subgiant HE 0233−0343, [Fe/H] = −4.7. We also revised the value for the star SMSS J1605−1443, [Fe/H] = −6.2, turning a lower limit into a value. Our main results are the following:

– For the three cool giants SMSS J0313−6708, SMSS J1605−1443, and SDSS J1313−0019, we derive a ^{12}C/^{13}C measurement, while for the two warm unevolved stars we provide a measurement for HE 0233−0343 and a lower limit for the dwarf HE 1327−2326. Measurements or limits are all in the range $39 < {}^{12}\mathrm{C}/{}^{13}\mathrm{C} < 100$, with a monotonic decrease going from the more metal-poor stars to the less metal-poor ones. The values derived for the ^{12}C/^{13}C ratio provide evidence of mixing between the He- and H-burning layers in the progenitors and a primary production of ^{13}C at the dawn of chemical evolution.
– For the CEMP-no dwarf stars with ^{12}C/^{13}C values in the literature, we find that very low isotopic values, even close to the CNO cycle equilibrium value, are common. In particular, they are also found in a few dwarfs. Both the literature

$^{12}C/^{13}C$ values and those obtained here show a monotonic decrease, reaching the lowest values at metallicities in the range [Fe/H] $\approx -4, -3$. This could mark a real difference between the progenitor ^{3}C pollution captured by stars with different metallicities. In particular, the decrease in the $^{12}C/^{13}C$ values with metallicity could reflect an increase in ^{13}C production by less massive stars (Limongi & Chieffi 2012).

– The ESPRESSO spectrum of HE 1327-2326 shows a hint of a Ba II line. If present, the abundance would be [Ba/Fe] = 1.3, making HE 1327-2326 the CEMP-no star with the highest barium abundance. Such an abundance violates the [Ba/Fe] < 0.0 criterion since HE 1327-2326 also has a carbon abundance characteristic of the CEMP-no stars. Indeed, there is a small group of CEMP-no stars with measured Sr values, of which four also have Ba measurements. The existence of this group of stars within the CEMP-no category indicates a very early synthesis of n-capture elements.
– A general correlation between $^{12}C/^{13}C$ values and Li abundance holds. Since the fragile Li is burned in the mixing process, low carbon isotopic ratios are generally associated with the largest Li depletions (Takeda et al. 2019). This is not observed in our stars, and Li depletion is observed for relatively high $^{12}C/^{13}C$ values, suggesting that neither mixing in the progenitor nor the CEMP-no nature of the stars is responsible for the Li depletion.

The study of the isotope ratio in low-mass halo stars has revealed the presence of significant synthesis of ^{13}C in the most massive stars of the very first stellar generations that contaminated the gas from which they formed. A synthesis that can only occur through the mixing of the helium and hydrogen burning layers, thus providing important information on the structure of the first stars. Future observations will have to ascertain how the values observed in low metallicity stars can be traced back to the high values observed in stars with solar abundances.

Acknowledgements. P.M. acknowledges important discussions with Marco Limongi about the ^{13}C production by massive zero metal stars. D.A. also acknowledges financial support from the Spanish Ministry of Science and Innovation (MICINN) under the 2021 Ramón y Cajal program MICINN RYC2021-032609. E.C. acknowledges support from the French National Research Agency (ANR) funded project Pristine (ANR-18-CE31-0017). J.I.G.H., C.A.P., A.S.M. and R.R. acknowledge financial support from the Spanish Ministry of Science and Innovation (MICINN) project PID2020-117493GB-I00. M.R.Z.O. acknowledges financial support from the Spanish Ministry of Science and Innovation through project PID2019-109522GB-C51. A.S.M. acknowledges financial support from the Spanish Ministry of Science and Innovation (MICINN) under 2018 Juan de la Cierva program IJC2018-035229-I. A.S.M. acknowledges financial support from the Government of the Canary Islands project ProID2020010129. F.P.E., C.L.O., and T.M.S. would like to acknowledge the Swiss National Science Foundation (SNSF) for supporting research with ESPRESSO through the SNSF grants nr. 140649, 152721, 166227, 184618, and 193689. The ESPRESSO Instrument Project was partially funded through SNSF's FLARE Programme for large infrastructures. D.M. is also supported by the INFN PD51 INDARK grant. This work was financed by FCT - Fundação para a Ciência e a Tecnologia under projects UIDB/04434/2020 & UIDP/04434/2020, CERN/FIS-PAR/0037/2019, PTDC/FIS-AST/0054/2021, PTDC 2022.04048(Phi in the Sky). C.J.M. also acknowledges FCT and POCH/FSE (EC) support through Investigador FCT Contract 2021.01214.CEECIND/CP1658/CT0001. M.T.M. acknowledges the support of the Australian Research Council through Future Fellowship grant FT180100194.

References

Aguado, D. S., Allende Prieto, C., González Hernández, J. I., Rebolo, R., & Caffau, E. 2017, A&A, 604, A9
Aguado, D. S., González Hernández, J. I., Allende Prieto, C., & Rebolo, R. 2018, ApJ, 852 L20
Aguado, D. S., González Hernández, J. I., Allende Prieto, C., & Rebolo, R. 2019, ApJ, 874, L21
Aguado, D., Molaro, P., Caffau, E., et al. 2022, A&A, 668, A86
Aguado, D. S., Caffau, E., Molaro, P., et al. 2023, A&A, 669, L4
Allen, D. M., Ryan, S. G., Rossi, S., Beers, T. C., & Tsangarides, S. A. 2012, A&A, 548, A34
Allende Prieto, C., Beers, T. C., Wilhelm, R., et al. 2006, ApJ, 636, 804
Allende Prieto, C., Fernández-Alvar, E., Aguado, D. S., et al. 2015, A&A, 579, A98
Almusleh, N. A., Taani, A., Özdemir, S., et al. 2021, Astron. Nachr., 342, 625
Aoki, W., Norris, J. E., Ryan, S. G., Beers, T. C., & Ando, H. 2002, ApJ, 567, 1166
Aoki, W., Norris, J. E., Ryan, S. G., et al. 2004, ApJ, 608, 971
Aoki, W., Frebel, A., Christlieb, N., et al. 2006, ApJ, 639, 897
Asplund, M., Amarsi, A. M., & Grevesse, N. 2021, A&A, 653, A141
Ayres, T. R., Lyons, J. R., Ludwig, H. G., Caffau, E., & Wedemeyer-Böhm, S. 2013, ApJ, 765, 46
Beers, T. C., & Christlieb, N. 2005, ARA&A, 43, 531
Beers, T. C., Preston, G. W., & Shectman, S. A. 1985, AJ, 90, 2089
Beers, T. C., Flynn, C., Rossi, S., et al. 2007, ApJS, 168, 128
Bessell, M. S., & Norris, J. 1984, ApJ, 285, 622
Bonifacio, P., Molaro, P., Beers, T. C., & Vladilo, G. 1998, A&A, 332, 672
Bonifacio, P., Caffau, E., Spite, M., et al. 2015, A&A, 579, A28
Bonifacio, P., Caffau, E., Spite, M., et al. 2018, A&A, 612, A65
Botelho, R. B., Milone, A. d. C., Meléndez, J., et al. 2020, MNRAS, 499, 2196
Bromm, V., & Loeb, A. 2003, Nature, 425, 812
Caffau, E., Bonifacio, P., François, P., et al. 2016, A&A, 542, A51
Caffau, E., Bonifacio, P., Sbordone, L., et al. 2013, A&A, 560, A71
Caffau, E., Bonifacio, P., Spite, M., et al. 2016, A&A, 595, L6
Carollo, D., Beers, T. C., Bovy, J., et al. 2012, ApJ, 744, 195
Chamberlain, J. W., & Aller, L. H. 1951, ApJ, 114, 52
Chiappini, C., Ekström, S., Meynet, G., et al. 2008, A&A, 479, L9
Christlieb, N., Gustafsson, B., Korn, A. J., et al. 2004, ApJ, 603, 708
Crossfield, I. J. M., Lothringer, J. D., Flores, B., et al. 2019, ApJ, 871, L3
Dearborn, D. S. P., Lambert, D. L., & Tomkin, J. 1975, ApJ, 200, 675
Deng, L.-C., Newberg, H. J., Liu, C., et al. 2012, Res. Astron. Astrophys., 12, 735
Ezzeddine, R., Rasmussen, K., Frebel, A., et al. 2020, ApJ, 898, 150
Frebel, A., & Norris, J. E. 2015, ARA&A, 53, 631
Frebel, A., Aoki, W., Christlieb, N., et al. 2005, Nature, 434, 871
Frebel, A., Collet, R., Eriksson, K., Christlieb, N., & Aoki, W. 2008, ApJ, 684, 588
Frebel, A., Chiti, A., Ji, A. P., Jacobson, H. R., & Placco, V. M. 2015, ApJ, 810, L27
Frebel, A., Ji, A. P., Ezzeddine, R., et al. 2019, ApJ, 871, 146
Frischknecht, U., Hirschi, R., Pignatari, M., et al. 2016, MNRAS, 456, 1803
Fu, X., Bressan, A., Molaro, P., & Marigo, P. 2015, MNRAS, 452, 3256
García Pérez, A. E., Christlieb, N., Ryan, S. G., et al. 2008, Phys. Scrip., 133, 014036
González Hernández, J. I., Aguado, D. S., Allende Prieto, C., Burgasser, A. J., & Rebolo, R. 2020, in XIV.0 Scientific Meeting (virtual) of the Spanish Astronomical Society, 142
Goto, M., Usuda, T., Takato, N., et al. 2003, ApJ, 598, 1038
Halfen, D. T., Woolf, N. J., & Ziurys, L. M. 2017, ApJ, 845, 158
Hansen, T., Hansen, C. J., Christlieb, N., et al. 2014, ApJ, 787, 162
Hansen, T., Hansen, C. J., Christlieb, N., et al. 2015, ApJ, 807, 173
Hansen, C. J., Nordström, B., Hansen, T. T., et al. 2016, A&A, 588, A37
Heger, A., & Woosley, S. 2020, Mem. Soc. Astron. Ital., 91, 58
Iben, I., & Renzini, A. 1984, Phys. Rep., 105, 329
Ishigaki, M., Tominaga, N., Kobayashi, C., & Nomoto, K. 2014, ApJ, 792, L32
José, J., & Hernanz, M. 1998, ApJ, 494, 680
Keller, S. C., Schmidt, B. P., Bessell, M. S., et al. 2007, PASA, 24, 1
Keller, S. C., Skymapper Team, & Aegis Team. 2012, ASP Conf. Ser., 458, 409
Keller, S. C., Bessell, M. S., Frebel, A., et al. 2014, Nature, 506, 463
Kobayashi, C., Karakas, A. I., & Lugaro, M. 2020a, ApJ, 900, 179
Kobayashi, C., Leung, S.-C., & Nomoto, K. 2020b, ApJ, 895, 138
Kurucz, R. L. 2005, Mem. Soc. Astron. Ital., 8, 14
Lambert, D. L., & Sneden, C. 1977, ApJ, 215, 597
Limongi, M., & Chieffi, A. 2012, ApJS, 199, 38
Limongi, M., & Chieffi, A. 2018, ApJS, 237, 13
Limongi, M., Chieffi, A., & Bonifacio, P. 2003, ApJ, 594, L123
Maeder, A., Meynet, G., & Chiappini, C. 2015, A&A, 576, A56
Masseron, T., Johnson, J. A., Plez, B., et al. 2010, A&A, 509, A93
Masseron, T., Johnson, J. A., Lucatello, S., et al. 2012, ApJ, 751, 14
Masseron, T., Plez, B., Van Eck, S., et al. 2014, A&A, 571, A47

Matsuno, T., Aoki, W., Suda, T., & Li, H. 2017, PASJ, 69, 24
Meynet, G., Ekström, S., & Maeder, A. 2006, A&A, 447, 623
Molaro, P. 2003, ASP Conf. Ser., 304, 221
Molaro, P., & Bonifacio, P. 1990, A&A, 236, L5
Molaro, P., & Castelli, F. 1990, A&A, 228, 426
Molaro, P., Centurión, M., D'Odorico, V., & Péroux, C. 2004, in Origin and Evolution of the Elements, eds. A. McWilliam, & M. Rauch (Cambridge: Cambridge University Press), 39
Mucciarelli, A., Monaco, L., Bonifacio, P., et al. 2022, A&A, 661, A153
Nomoto, K., Kobayashi, C., & Tominaga, N. 2013, ARA&A, 51, 457
Nordlander, T., Amarsi, A. M., Lind, K., et al. 2017, A&A, 597, A6
Nordlander, T., Bessell, M. S., Da Costa, G. S., et al. 2019, MNRAS, 488, L109
Norris, J. E., Ryan, S. G., & Beers, T. C. 1997, ApJ, 489, L169
Norris, J. E., Bessell, M. S., Yong, D., et al. 2013a, ApJ, 762, 25
Norris, J. E., Yong, D., Bessell, M. S., et al. 2013b, ApJ, 762, 28
Pagnini, G., Salvadori, S., Rossi, M., et al. 2023, MNRAS, 521, 5699
Pepe, F., Cristiani, S., Rebolo, R., et al. 2013, The Messenger, 153, 6
Pepe, F., Cristiani, S., Rebolo, R., et al. 2021, A&A, 645, A96
Plez, B., & Cohen, J. G. 2005, A&A, 434, 1117
Rockosi, C. M., Lee, Y. S., Morrison, H. L., et al. 2022, ApJS, 259, 60
Romano, D. 2022, A&ARv, 30, 7
Romano, D., & Matteucci, F. 2003, MNRAS, 342, 185
Sbordone, L. 2005, Mem. Soc. Astron. Ital., 8, 61
Sbordone, L., Bonifacio, P., Caffau, E., et al. 2010, A&A, 522, A26
Sivarani, T., Beers, T. C., Bonifacio, P., et al. 2006, A&A, 459, 125
Spite, M., Cayrel, R., Hill, V., et al. 2006, A&A, 455, 291
Spite, M., Caffau, E., Bonifacio, P., et al. 2013, A&A, 552, A107
Spite, M., Spite, F., & Barbuy, B. 2021, A&A, 652, A97
Starkenburg, E., Shetrone, M. D., McConnachie, A. W., & Venn, K. A. 2014, MNRAS, 441, 1217
Starkenburg, E., Martin, N., Youakim, K., et al. 2017, MNRAS, 471, 2587
Starrfield, S., Truran, J. W., Sparks, W. M., & Kutter, G. S. 1972, ApJ, 176, 169
Takeda, Y., Omiya, M., Harakawa, H., & Sato, B. 2019, PASJ, 71, 119
Tominaga, N., Umeda, H., & Nomoto, K. 2007, ApJ, 660, 516
Tominaga, N., Iwamoto, N., & Nomoto, K. 2014, ApJ, 785, 98
Umeda, H., & Nomoto, K. 2003, Nature, 422, 871
Umeda, H., & Nomoto, K. 2005, ApJ, 619, 427
Vrug, A., ter Braak, C., Dicks, C., et al. 2009, Int. J. Nonlinear Sci. Numer. Simulation, 10, 273:290
Yan, Y. T., Henkel, C., Kobayashi, C., et al. 2023, A&A, 670, A98
Yanny, B., Rockosi, C., Newberg, H. J., et al. 2009, AJ, 137, 4377
York, D. G., Adelman, J., Anderson, John E., J., et al. 2000, AJ, 120, 1579
Zafar, T., Centurión, M., Péroux, C., et al. 2014, MNRAS, 444, 744
Zepeda, J., Beers, T. C., Placco, V. M., et al. 2023, ApJ, 947, 23

[1] INAF-Osservatorio Astronomico di Trieste, Via G.B. Tiepolo 11, 34143 Trieste, Italy
e-mail: paolo.molaro@inaf.it
[2] Institute of Fundamental Physics of the Universe, Via Beirut 2, 34151 Trieste, Italy
[3] Instituto de Astrofísica de Canarias, Vía Láctea, 38205 La Laguna, Tenerife, Spain
[4] GEPI, Observatoire de Paris, Université PSL, CNRS, 5 Place Jules Janssen, 92190 Meudon, France
[5] Universidad de La Laguna, Departamento de Astrofísica, 38206 La Laguna, Tenerife, Spain
[6] Consejo Superior de Investigaciones Científicas, C. De Serrano 117, 28006 Madrid, Spain
[7] Centro de Astrobiología (CSIC-INTA), Carretera Ajalvir km 4, 28850 Torrejón de Ardoz, Madrid, Spain
[8] Département d'astronomie de l'Université de Genève, Chemin Pegasi 51, 1290 Versoix, Switzerland
[9] Instituto de Astrofísica e Ciências do Espaço, CAUP, Universidade do Porto, Rua das Estrelas, 4150-762, Porto, Portugal
[10] Departamento de Física e Astronomia, Faculdade de Ciências, Universidade do Porto, Rua Campo Alegre, 4169-007 Porto, Portugal
[11] Scuola Normale Superiore P.zza dei Cavalieri 7, 56126 Pisa, Italy
[12] Instituto de Astrofísica e Ciências do Espaço, Faculdade de Ciências da Universidade de Lisboa, Campo Grande, 1749-016 Lisboa, Portugal
[13] Centro de Astrofísica da Universidade do Porto, Rua das Estrelas, 4150-762 Porto, Portugal
[14] INFN, Sezione di Trieste, Via Valerio 2, 34127 Trieste, Italy
[15] INAF – Osservatorio Astrofisico di Torino, Via Osservatorio 20, 10025 Pino Torinese, Italy
[16] Physics Institute of University of Bern, Gesellschafts strasse 6, 3012 Bern, Switzerland
[17] Centre for Astrophysics and Supercomputing, Swinburne University of Technology, 13 John St, Hawthorn, Victoria 3122, Australia